Aquaporin 0 Modulates Lens Gap Junctions in the Presence of Lens-Specific Beaded Filament Proteins

Sindhu Kumari,[1] Junyuan Gao,[1] Richard T. Mathias,[1,2] Xiurong Sun,[1] Amizhdini Eswaramoorthy,[1] Nicholas Browne,[1] Nigel Zhang,[1] and Kulandaiappan Varadaraj[1,2]

[1]Department of Physiology and Biophysics, Stony Brook University, Stony Brook, New York, United States
[2]SUNY Eye Institute, Syracuse, New York, United States

Correspondence: Kulandaiappan Varadaraj, Department of Physiology and Biophysics, BST-6, Room # 165A, School of Medicine, Stony Brook University, NY 11794-8661, USA; kulandaiappan.varadaraj@stonybrook.edu.

Submitted: May 2, 2017
Accepted: October 23, 2017

Citation: Kumari S, Gao J, Mathias RT, et al. Aquaporin 0 modulates lens gap junctions in the presence of lens-specific beaded filament proteins. *Invest Ophthalmol Vis Sci*. 2017;58:6006–6019. DOI:10.1167/iovs.17-22153

Purpose. The objective of this study was to understand the molecular and physiologic mechanisms behind the lens cataract differences in Aquaporin 0-knockout-Heterozygous (AQP0-Htz) mice developed in C57 and FVB (lacks beaded filaments [BFs]) strains.

Methods. Lens transparency was studied using dark field light microscopy. Water permeability (P_f) was measured in fiber cell membrane vesicles. Western blotting/immunostaining was performed to verify expression of BF proteins and connexins. Microelectrode-based intact lens intracellular impedance was measured to determine gap junction (GJ) coupling resistance. Lens intracellular hydrostatic pressure (HP) was determined using a microelectrode/manometer system.

Results. Lens opacity and spherical aberration were more distinct in AQP0-Htz lenses from FVB than C57 strains. In either background, compared to wild type (WT), AQP0-Htz lenses showed decreased P_f (approximately 50%), which was restored by transgenic expression of AQP1 (TgAQP1/AQP0-Htz), but the opacities and differences between FVB and C57 persisted. Western blotting revealed no change in connexin expression levels. However, in C57 AQP0-Htz and TgAQP1/AQP0-Htz lenses, GJ coupling resistance decreased approximately 2.8-fold and the HP gradient decreased approximately 1.9-fold. Increased P_f in TgAQP1/AQP0-Htz did not alter GJ coupling resistance or HP.

Conclusions. In C57 AQP0-Htz lenses, GJ coupling resistance decreased. HP reduction was smaller than the coupling resistance reduction, a reflection of an increase in fluid circulation, which is one reason for the less severe cataract in C57 than FVB. Overall, our results suggest that AQP0 modulates GJs in the presence of BF proteins to maintain lens transparency and homeostasis.

Keywords: Aquaporin 0, gap junctions, beaded filaments, cataractogenesis, transparency

The eye lens is a transparent, avascular organ that is responsible for approximately 40% of the focusing power for vision in humans. Structurally, a single layer of cuboidal epithelial cells covers the anterior hemisphere of the lens. Fiber cells constitute the bulk of the lens. They differentiate from the equatorial epithelial cells, elongate, and greatly change their compliment of membrane and cytoplasmic proteins. Approximately 15% of the distance into the lens, fiber cells undergo a second stage of maturation that eliminates cellular organelles and generates C-terminal cleavage of most membrane proteins, including Aquaporin 0 (AQP0)[1,2] and gap junction (GJ) connexins (Cx).[1–8] These modifications reduce light scattering and can allow central fibers to survive for the lifetime of the organism.[9,10] In addition, these events help to adjust the refractive index gradient[2,11,12] and biomechanics[13] of the lens for proper focusing of light from nearby or far objects. The mammalian ocular lens contains approximately 66% water and approximately 33% proteins. To adjust the refractive index, lens fiber cell cytosolic protein concentration and free water content are maintained in a reciprocal gradient from the cortex to the nucleus.

Since the lens is avascular, to procure nourishment and dispose of metabolic waste, it creates a microcirculation involving water channels, ion transporters, and cotransporters.[14–16] Intercellular GJ channels constituted by Cx membrane proteins form epithelial-to-epithelial, fiber-to-fiber, and epithelial-to-fiber cell connections at the plasma membrane.[17–20] Small molecules, such as ions, metabolites, and second messengers, pass between two such connected cells[21,22] and aid in intercellular communication. Three major GJ channel proteins are present in the lens. Cx43 (*α1* gene) and Cx50 (*α8* gene) are expressed in the epithelial cells; Cx46 (*α3* gene) and Cx50 are expressed in the fiber cells.[23,24] Along with GJ channels, lens water pores or aquaporin (AQPs)[2,11–16,25–34] namely AQP0, AQP1, and AQP5 have significant roles in lens microcirculation and homeostasis. In a simplified version of the microcirculation model, sodium ions enter the extracellular spaces at the anterior and posterior poles of the lens.[14–16,30] As the extracellular sodium flows toward the central part of the lens, the ions enter the fiber cells down their electrochemical potential across the fiber cell membranes. Once in the intracellular compartment, the flow reverses direction and moves from fiber cell to fiber cell through GJs back toward the lens equatorial surface. The Na-K-ATPase expressed in equatorial epithelial cells[35] pumps the sodium out. Through the processes of osmosis and hydrostatic pressure (HP), water

follows the circulation of sodium.[36–38] The inward extracellular fluid flow carries nutrients and antioxidants to central fiber cells (reviewed previously[15]) while the outward intracellular fluid flow carries waste products, such as lactic acid,[39,40] from central fibers to surface cells that can eliminate them.

Yorio et al.[41] have shown active oxidative metabolism in the outer cortical region of the lens and glycolysis in the central nucleus. Experimental evidence shows that lens center has an acidic pH (6.81) compared to the outer cortex (7.2).[39,40] The presence of low pH in the center of the lens is due partly to the accumulation of lactic acid as a result of anaerobic glycolysis. GJ channels appear to serve as the cell-to-cell outflow conduit for the intracellular leg of the lens microcirculatory system,[16] which carries lactic acid and possibly other waste products to surface cells where they are eliminated.

AQPs[13,25–29,42] and GJ channels[16] have significant roles in lens homeostasis. In vivo and in vitro studies were conducted by different groups to find out whether AQP0 has a role in GJ regulation producing mixed results. An in vivo study on an AQP0 knockout mouse model developed in the FVB strain that does not express beaded filaments (BFs) due to a mutation in the *CP49* gene showed that 50% reduction in AQP0 does not alter lens GJ coupling. In vitro studies indicated that AQP0 facilitates GJ coupling; the cell-to-cell adhesion (CTCA) function of AQP0 might have promoted Cx50 GJ coupling.[29,43] Moreover, several investigators have shown the possible interaction of AQP0 with lens Cx[17,44,45] and cytoskeletal proteins (e.g., BF proteins CP49 and filensin[46,47]). Therefore, the role of AQP0 in lens GJ regulation is an open question. The difference in the results between in vitro and in vivo studies on the effect of AQP0 on GJ coupling could be due to several factors, such as the amount of AQP0 present, Cx expression levels or lack of other regulatory components in an in vitro environment.

AQP0 is the most abundantly expressed membrane protein in the plasma membranes of fiber cells, constituting approximately 44.8% of the total membrane proteins in the lens. Scientists were intrigued by the prolific expression of AQP0 and sought to determine the role(s) of this protein in the lens. Mutations in AQP0 result in autosomal dominant lens cataract in mice[48–53] as well as humans.[29,54,55] In vitro and in vivo studies demonstrated that AQP0 functions as a water channel[25,27,56–58] and a CTCA molecule,[26,28,43,59–61] both of which are important in maintaining lens transparency,[26–28,62] refractive index gradient,[2,11] biomechanics,[13] and homeostasis.[14–16,30] AQP0 interacts with other membrane proteins, such as Cx,[17,44,63] and lens-specific cytoskeletal intermediate BF proteins CP49 (phakinin) and filensin (CP115).[46] We suggested the involvement of BFs in the anchorage and distribution of AQP0 at the plasma membrane.[2] Alteration in refractive index gradient, and increased spherical aberration and severity of cataract were observed in AQP0-heterozygous (Htz) FVB strain mice that lack BFs compared to similar lenses of mice from the C57 strain, which expresses BF proteins. It also has been reported that lack of BFs caused alteration in lens biomechanical properties.[64,65]

Reduction, mutation, or loss of AQP0 and GJ channel proteins, which are critical for the microcirculation, disrupts homeostatic balance and causes lens opacities.[23–25,27,66,67] It has been shown that AQP0 knockout (AQP0-KO) mice established in the FVB strain develop more severe lens cataracts compared to those in the C57 strain, suggesting the involvement of BFs with lens transparency. Mutations and KO of lens protein genes in the 129/SvJae mouse strain also resulted in a more severe cataract phenotype than those in the C57 strain.[68,69] A previous study investigated lenses of AQP0-Htz, TgAQP1/AQP0-Htz, and wild type (WT) mice in FVB background; there was no significant difference in GJ resistance or HP among the three types of lenses.[30] To understand the molecular and physiologic mechanisms underlying the difference in lens cataract phenotypes observed in the two different mouse strains, we investigated AQP0 and GJ channel functions in WT, AQP0-Htz, and TgAQP1/AQP0-Htz[26,28] mouse lenses in C57 background and compared them to those in similar genotypes from FVB.

Materials and Methods

Animals

The following mouse models were used: WT mouse strains FVB/N (FVB; Charles River Laboratories, Wilmington, MA, USA) and C57BL/6J (C57; Jackson Laboratories, Bar Harbor, ME, USA), AQP0 heterozygous in both strains (AQP0-Htz-FVB, AQP0-Htz-C57), and AQP0-Htz mouse expressing AQP1 in the fiber cells in both strains (transgenic, TgAQP1/AQP0-Htz-FVB; TgAQP1/AQP0-Htz-C57). Animal procedures were performed according to the ARVO Statement for the Use of Animals in Ophthalmic and Vision Research, the National Institutes of Health (NIH; Bethesda, MD, USA) "Guide for the Care and Use of Laboratory Animals" and protocols approved by Stony Brook University Animal Care and Use Committee.

Originally, the AQP0-KO mouse model was established in a mixed background of 129S5 and C57BL/6J-albino.[27] We transferred it to the FVB strain by backcrossing the AQP0-KO with WT FVB for more than 25 generations.[26] Since FVB mice[70] do not express CP49, a constituent of lens-specific BFs, due to a deletion mutation in the *CP49* gene, the AQP0-KO mouse model developed in the FVB background[26] was backcrossed with C57 for more than 25 generations to transfer the knockout genotype in this strain. Genotyping using PCR primers described by Alizadeh et al.[71] (primer set I) and Simirskii et al.[70] (primer set II) were used to distinguish the genotypes. These procedures were followed to ascertain that the data collected on lens fiber cell water permeability (P_f), CTCA, GJ coupling resistance and intracellular HP are strain-specific for data comparison.

Initially, we developed TgAQP1/AQP0-Htz in the FVB mouse strain.[26] Restoring membrane P_f in TgAQP1/AQP0-Htz partially restored lens transparency in FVB.[26,28] To see whether restoring P_f in the presence of BFs alter the outcome, we developed TgAQP1/AQP0-Htz in the C57 strain. For this, TgAQP1$^{+/+}$ /AQP0$^{-/-}$ in FVB was backcrossed with C57 WT for more than 25 generations and genotyped using PCR primers described by Simirskii et al.[70] and Alizadeh et al.[71] Strain transfer and genotyping were done to ensure that the data we collected using these mice were from the C57 genetic background.

Lens Transparency and Spherical Aberration

Lenses from 2-month-old mice (5 lenses/group) were dissected out in prewarmed (37°C) mammalian physiologic saline. Images were captured under the same lighting and imaging conditions using a dark field Zeiss binocular microscope attached with a Olympus digital camera.[11] Lens transparency was quantified using the dark field lens images, which were converted to gray scale (Adobe Photoshop 9; Adobe Systems, San Jose, CA, USA) and processed using ImageJ software (NIH). An area from the lens image was drawn out as a square box to analyze and plot profile function and was selected to create values of pixel brightness intensity. Sigma Plot 10 software was used to plot a histogram for pixel brightness intensity data.

Qualitative assessment of lens spherical aberration was performed using dark field optical grid focusing.[11] A copper

Investigative Ophthalmology & Visual Science

electron microscope specimen grid was imaged through a whole lens placed on it. Quality of the grid lines focused was evaluated for light scatter and defocusing effects due to refractive index gradient alteration and spherical aberration.

Western Blotting

Fiber cell membrane proteins were extracted using 4M-urea-buffer (4 mM Tris-HCl, pH 8.0; 5 mM EDTA, 4M Urea) from the lenses of WT, AQP0-Htz, and TgAQP1/AQP0-Htz in C57 as well as WT and AQP0-Htz in FVB strains. For Western blotting, lens protein samples were resolved on 4% to 12% gradient NuPAGE gels (Invitrogen, Carlsbad, CA, USA). Broad range Kaleidoscope markers (Bio-Rad Laboratories, Hercules, CA, USA) were loaded to estimate the molecular sizes of the reactive bands. Proteins were transferred to a nylon membrane. Since the colored marker proteins do not bind to antibody and may fade during processing, positions of the molecular size standards were marked with a sharp pencil on the blot before removal of the blot from the gel. This step helped us to find out the relative molecular size of the protein band binding to the antibody. Western blotting was done as described.[72,73] Antibodies to CP49, filensin (from Paul G. FitzGerald, University of California-Davis, Davis, CA, USA), Cx43, Cx46, and Cx50 (Santa Cruz Biotechnology, Dallas, TX, USA) were used. Antibody binding was detected using alkaline phosphatase kit (Vector Laboratories, Burlingame, CA, USA).

Analysis of Localization of Lens AQP0 and BF Proteins CP49 and Filensin

Lenses from 2-month-old WT and AQP0-Htz mice were dissected out, fixed for 12 hours in 2% and 24 hours in 4% paraformaldehyde, and rinsed in PBS. Lenses were cryosectioned (14 µm thickness) using a cryomicrotome (Leica, Wetzlar, Germany) and sections were stored at −20°C. Cryosections were permeabilized (0.2% vol/vol Triton X-100) for 30 minutes at room temperature, blocked with normal goat serum, and treated with rabbit polyclonal antibody raised against AQP0 (Santa Cruz Biotechnology), and mouse monoclonal antibody against filensin or CP49 in appropriate dilutions using 5% (wt/vol) BSA in PBS. After overnight incubation and three washes in PBS, the slides were incubated with FITC conjugated goat anti-rabbit IgG or Texas Red conjugated goat anti-mouse IgG in PBS containing 5% BSA. The slides with the treated tissue sections were washed again in PBS, mounted in anti-fade Vectamount (Vector Laboratories) and viewed under an epifluorescent confocal microscope. Optimized Z-sectional digital images were acquired with a Zeiss Axiovert 200 inverted microscope equipped with AxioCam and Zeiss AxioVision 5 software (Carl Zeiss MicroImaging, Inc., Munich, Germany) and processed using Adobe Photoshop 9.0.

Lens Fiber Cell Membrane P_f Assay

Experiments for P_f measurement were performed using the rate of shrinking of fiber cell membrane vesicles, as described previously.[25,27,74] In brief, lens capsules were removed, outer cortex fiber cell bundles were isolated and fiber cell membrane vesicles were prepared. Each vesicle was incubated in hypertonic saline (450 mOsm), and the rate of shrinkage was imaged by digital video microscopy and P_f was calculated as described by Varadaraj et al.[25]

Lens GJ Coupling Measurement

Lenses from 2-month-old WT, AQP0-Htz, and TgAQP1/AQP0-Htz mice from C57 background were dissected out and mounted as described previously.[36] In brief, eyes were removed from euthanized mice and placed in a Sylgard-lined petri dish filled with normal Tyrode solution, pH 7.4 (in mM: 137.7 NaCl, 2.3 NaOH, 5.4 KCl, 2 $CaCl_2$, 1 $MgCl_2$, 5 HEPES, and 10 glucose). To mount the lens in the perfusion chamber for impedance studies, the anterior segment of the eye, cornea, and iris were dissected out. The optic nerve was removed from the posterior side of the eye and the sclera was cut into four flaps through the hole created while cutting the optic nerve. The lens was pinned to the Sylgard base present at the bottom of a perfusion chamber containing normal Tyrode solution. The perfusion chamber with lens was attached to a microscope stage. Normal Tyrode's solution was used to perfuse the lens.

Measurement of lens GJ coupling resistance was performed as described previously.[36] Briefly, a wide-band stochastic current was injected through a microelectrode that was inserted into a central fiber cell. A second microelectrode inserted into a peripheral fiber cell at a distance r (cm) from the center of a lens of radius a (cm) was used to record the induced voltage. Using a fast Fourier analyzer (Hewlett Packard, Palo Alto, CA, USA), the frequency domain impedance (induced voltage ÷ injected current) of the lens was recorded in real time. At high frequencies, the magnitude of the lens impedance asymptotes to the series resistance (R_S) which is due to all the GJs between the point of voltage recording and the lens surface. By measuring $R_S K\Omega$ at multiple depths into lenses of each type, then curve fitting the data with Equation 1, the underlying effective intracellular resistivities ($R_{DF}, R_{MF} K\Omega cm$) were determined. These effective resistivities were determined from the radial voltage drop, so they represent the radial component of GJ coupling resistance.

$$R_s(r) = \begin{cases} \frac{R_{DF}}{4\pi}\left(\frac{1}{r} - \frac{1}{a}\right) & b \le r \le a \\ \frac{R_{DF}}{4\pi}\left(\frac{1}{b} - \frac{1}{a}\right) + \frac{R_{MF}}{4\pi}\left(\frac{1}{r} - \frac{1}{b}\right) & 0 \le r \le b \end{cases} \quad (1)$$

Fiber cells transition from peripheral differentiating fibers (DF – outer cortex containing intact proteins) to central mature fibers (MF) at a radial location $b \cong 0.85a$, where $r\,cm$ is the radial distance from the lens center and $a\,cm$ is the lens radius. MF includes inner cortex, outer nucleus (both containing maturing fiber cells that undergo post-translational modifications [PTMs]) and inner nucleus (containing matured fiber cells). At inner cortex and outer nuclear regions of MF, the C-termini of Cx46 and Cx50 are cleaved gradually, resulting in a change in coupling resistance. The GJ coupling conductance per area of cell-to-cell radial contact can be estimated from the effective resistivities by:

$$G_{DF,MF} = \frac{1}{wR_{DF,MF}} \quad \frac{S}{cm^2} \quad (2)$$

where $w \cong 3x10^{-4} cm$ is the fiber cell width.

Lens Intracellular HP Measurements

Intracellular HP in intact lenses was measured as described by Gao et al.[36] Briefly, microelectrodes were pulled with a resistance in the range of 1.5 to 2 MΩ when filled with 3 M KCl. A microelectrode was inserted into the intact lens. The positive intracellular pressure of the fiber cell forced cytoplasm into the microelectrode tip causing an increase in resistance. Pressure was applied to the interior of the microelectrode until its resistance just returned to the value measured outside of the lens. This pressure was measured using a manometer. Recording was performed for four to five depths in each lens. Data from at least eight lenses were pooled for each genotype.

Investigative Ophthalmology & Visual Science

The average pressure gradient was estimated by curve-fitting Equation 3 to the pooled data.

$$p_i(r) = \begin{cases} p_i(b)\left(\frac{a^2-r^2}{a^2-b^2}\right) & b \le r \le a \\ p_i(b) + (p_i(0) - p_i(b))\left(\frac{b^2-r^2}{b^2}\right) & 0 \le r \le b \end{cases} \quad (3)$$

The quadratic r-dependence of pressure suggests the transmembrane entry of water into fiber cells essentially is uniform with depth into the lens.[36] The change in slope of the r-dependence at $r = b$ is thought to occur because the number of open GJ channels goes down in the MF relative to DF.

Statistical Analysis

SigmaPlot 10 software was used for Student's t-tests. P values ≤ 0.05 were considered significant.

Results

Genotyping, Protein Expression and Localization

Pups were genotyped to authenticate the presence or absence of CP49 deletion mutation (Fig. 1A). Two sets of PCR reactions were assembled and performed; the primers used were as described by Alizadeh et al.[71] (primer set I) and Simirskii et al.[70] (competitive PCR; primer set II). Primer set I amplified a 320-base pair (bp) segment for WT, AQP0-Htz, and TgAQP1/AQP0-Htz in the C57 strain. A 386-bp product was amplified for FVB indicating the presence of mutant CP49 alleles. Primer set II[70] amplified a 205-bp segment for all except FVB (Fig. 1A), which produced a 347-bp amplicon indicating the presence of mutant CP49 alleles; the 205 bp amplicon confirmed the absence of CP49 deletion mutation. These results ensured the selection of the desired genotypes for experiments and for appropriate analyses of the collected data.

Total membrane proteins of WT, AQP0-Htz, and TgAQP1/AQP0-Htz mice in C57 or FVB background were prepared and Western blotting was performed. Protein expression was confirmed using antibodies to BF proteins (CP49 or filensin). Western blot analyses showed binding of the antibodies to the respective polypeptide bands for filensin (approximately 95 kDa; arrow, Fig. 1B) and CP49 (approximately 49 kDa; arrow, Fig. 1B) in WT, AQP0-Htz, and TgAQP1/AQP0-Htz mouse lenses of C57 background. In FVB, there was no detectable immunoreaction with CP49 antibody. However, there was low level binding due to a low level of filensin; absence of CP49 causes instability of the filensin polypeptide[71,75] despite FVB expressing filensin transcripts.[38] These experiments showed the absence of BFs in FVB lenses in parallel with the presence of both BF proteins in C57 lenses.

After confirming the presence of BF proteins in C57 lens membranes by Western blotting, we tested whether AQP0 and BF proteins localize at the plasma membrane. Lens cryosections of WT, AQP0-Htz, and TgAQP1/AQP0-Htz mice in C57 and FVB genetic backgrounds were immunostained using AQP0, CP49, and filensin antibodies (Figs. 1C, 1D). In the C57 genetic background, fiber cell membranes of WT (Fig. 1C), AQP0-Htz (Fig. 1C), and TgAQP1/AQP0-Htz (Fig. 1C) displaying red indicate the binding of AQP0 antibody. Membrane images in green indicate binding of filensin or CP49 antibodies. In Figure 1C, the images at the bottom indicate AQP1 expression at the plasma membrane. In the FVB genetic background, fiber cell membranes of WT, AQP0-Htz, and TgAQP1/AQP0-Htz displaying red indicate the binding of AQP0 antibody (Fig. 1D). Membrane images in Figure 1D did not show any specific binding of either filensin or CP49 antibodies for all genotypes tested. In Figure 1D, green indicates the AQP1-EGFP expression at the fiber cell membrane.

Lens Transparency

Lens transparency was assessed for WT, AQP0-Htz, and TgAQP1/AQP0-Htz in C57 and FVB genetic backgrounds using light microscopic images of 2-month-old lenses. Compared to AQP0-Htz and TgAQP1/AQP0-Htz lenses in the C57 strain, those of AQP0-Htz and TgAQP1/AQP0-Htz in the FVB strain showed relatively higher light scattering (Fig. 2A, top row). While AQP0-Htz and TgAQP1/AQP0-Htz lenses in both backgrounds focused the grid lines poorly as a result of light scattering and spherical aberration, the severity was more pronounced in the lenses in the FVB than those in the C57 strains (Fig. 2A, bottom row). Figures 2B and 2C show lenses of WT, AQP0-Htz, and TgAQP1/AQP0-Htz in C57 and FVB genetic backgrounds (five lenses each) used for quantifying lens transparency. Figure 2D shows quantification of lens transparency, which is calculated on the basis of it being inversely proportional to pixel brightness intensity. While WT lenses were clear with the lowest pixel brightness that translates to very low light scattering, AQP0-Htz and TgAQP1/AQP0-Htz lenses showed more pixel brightness and higher levels of light scattering (Figs. 2A–D). Lenses of AQP0-Htz and TgAQP1/AQP0-Htz mice in the FVB strain showed significant increase in light scattering (marked with an asterisk in Fig. 2D) and, hence, statistically significant reduction in lens transparency compared to their counterparts in the C57 strain.

Lens Fiber Cell Membrane Water Permeability (P_f)

The P_f of WT, AQP0-Htz, TgAQP1/AQP0-Htz in C57 and FVB genetic backgrounds was studied using lens cortical fiber cell membrane vesicles. P_f was calculated by the rate of shrinking of each vesicle when subjected to a hypertonic bath solution. Fiber cell membrane vesicles of WT expressing AQP0 in C57 and FVB genetic backgrounds (Fig. 3; Table 1) had an average P_f of 40 ± 10 and 38 ± 8 μm/s, respectively, which was not affected by exposure to $HgCl_2$ (C57, 43 ± 11 μm/s; FVB, 42 ± 10 μm/s; Table 1), an inhibitor of AQP1.[25,76,77] Loss of 50% of AQP0 in AQP0-Htz mouse lens fiber cell membranes of C57 and FVB resulted in a P_f of approximately 20 ± 11 and 21 ± 10 μm/s, respectively, which also were unaffected by $HgCl_2$ (C57, 22 ± 10 μm/s; FVB, 22 ± 8 μm/s; Table 1) as seen for the WT. The fiber cell membrane vesicles of transgenic AQP1 mice (TgAQP1/AQP0-Htz) showed >3-fold increase in P_f (C57, 63 ± 14 μm/s; FVB, 62 ± 13 μm/s), owing to the presence of the highly efficient AQP1, compared to those of AQP0-Htz lens and >1.5-fold increase compared to those of WT ($P < 0.001$; Fig. 3; Table 1). The increased P_f in TgAQP1/AQP0-Htz lens fiber cell was partially inhibited (C57: 36 ± 8 μm/s; FVB: 35 ± 11 μm/s) by $HgCl_2$ (Fig. 3; Table 1). Previously, we reported that transgenic expression of AQP1 in the fiber cells of AQP0-Htz in the FVB strain restored P_f that was lost due to the KO of native AQP0, but lens transparency was not restored completely.[26,28] In our study in the C57 strain, even though lens transparency of the transgenic model showed significant improvement compared to that in the FVB strain, P_f did not differ significantly from that in the FVB background (Fig. 3; Table 1).

Loss of One Copy of AQP0 in C57 Mouse Lenses Results in Decreased GJ Coupling Resistance and Intracellular HP

Several investigations on mutant or KO genes in mouse lenses have revealed that an increase in GJ coupling resistance leads to an increase in intracellular HP.[36,78–82] However, loss of 50%

Investigative Ophthalmology & Visual Science

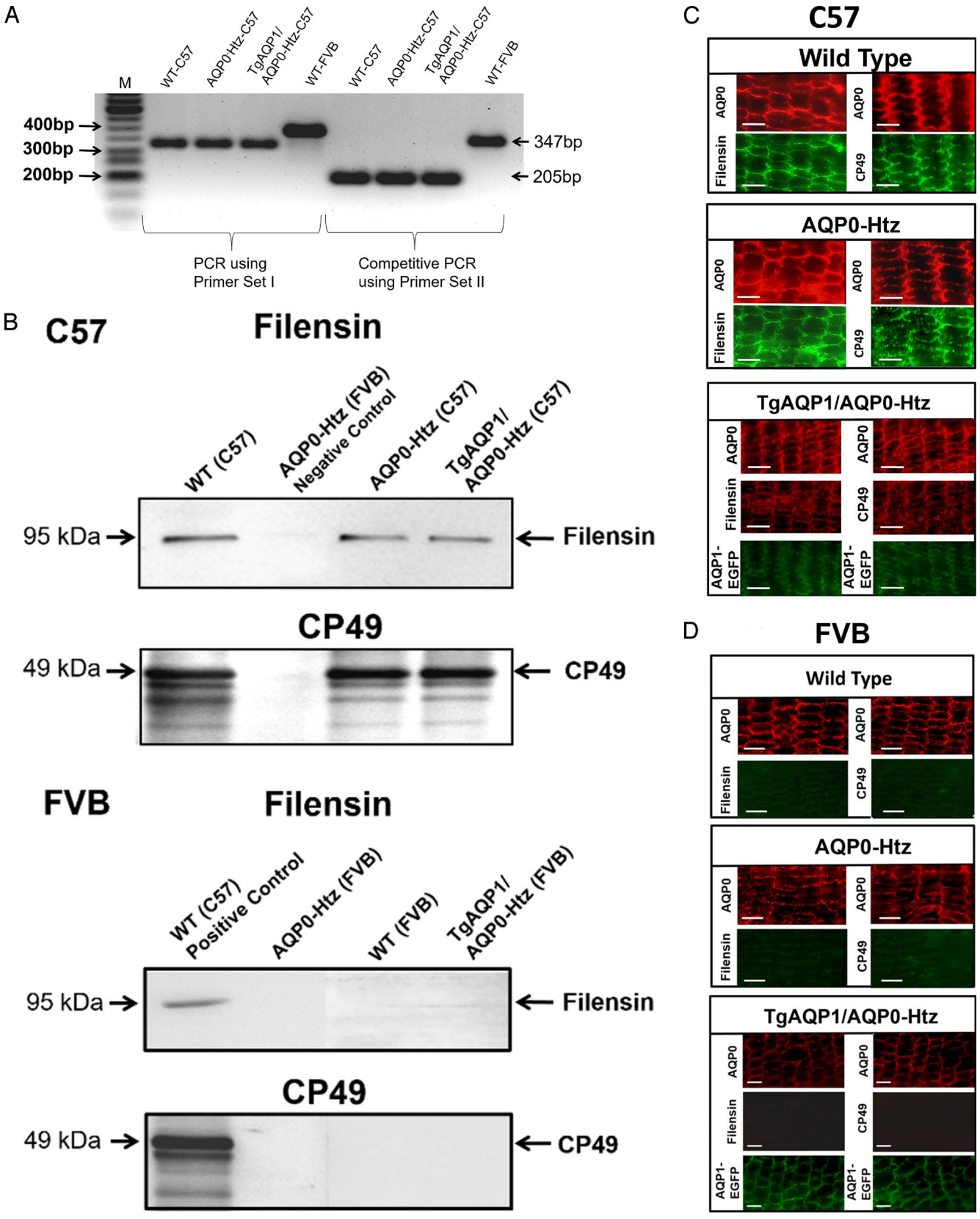

Figure 1. (**A**) Genotyping to confirm the presence or absence of CP49 natural mutation. PCR using primers published by Alizadeh et al.[71] (Primer set I); 320 bp, indicates the presence of intact CP49 allele; 386 bp, shows the presence of mutant CP49 allele. Competitive PCR as described by Simirskii et al.[70] (Primer set II); 205-bp points to the presence of intact CP49 allele; 347-bp indicates the presence of mutant CP49 allele. M, Marker (50-bp Ladder). (**B**) Western blotting of filensin and CP49 in different genotypes as indicated. *Arrows* indicate immunoreactive bands. Blots treated with: filensin antibody (*arrow*, filensin, approximately 95 kDa) or CP49 antibody (*arrow*, CP49, approximately 49 kDa). (**C**) Immunostaining of AQP0 and BF proteins in C57 genetic background lenses: WT, AQP0-Htz, and TgAQP1/AQP0-Htz. Cryosections of 2-month-old lenses were

Investigative Ophthalmology & Visual Science

immunostained using AQP0 and BF protein antibodies. For anti-AQP0, Texas Red-conjugated secondary antibody was used; for anti-filensin or anti-CP49-treated slides FITC-conjugated secondary antibody was used. Sections were imaged using Zeiss confocal microscope. (**D**) Immunostaining of AQP0 and BF proteins in FVB genetic background lenses: WT, AQP0-Htz, and TgAQP1/AQP0-Htz. Cryosections of 2-month-old lenses in were immunostained as described for Figure 1C. Lowermost images in C and D show AQP1-EGFP fluorescence. Sections were imaged using Zeiss confocal microscope. *Scale bar*: 12 μm.

of AQP0[30] in the FVB mice that lack BFs, or expression of a mutated AQP0 protein (e.g., *Cat*^{FR} mouse)[25] did not alter lens GJ coupling resistance or intracellular HP. These results motivated us to test whether there is any change in GJ coupling resistance and intracellular HP in AQP0-Htz or TgAQP1/AQP0-Htz in the C57 strain compared to the WT.

Data from our experiments in C57 background showed that there are significant differences in the values of series resistance (R_S) and coupling conductance (Figs. 4A, 4B; Table 2) in AQP0-Htz, and TgAQP1/AQP0-Htz mouse lenses compared to the WT lenses. In AQP0-Htz and TgAQP1/AQP0-Htz mice, coupling conductance per area of cell-to-cell contact of differentiating fibers was approximately 0.8 S/cm^2 for all types of lenses; however, the coupling conductance (G_i) of mature fibers increased dramatically in Htz lenses. It was 0.54 S/cm^2 in WT lenses but increased to 1.53 S/cm^2 in AQP0-Htz and 1.41 in TgAQP1/AQP0-Htz lenses (Table 2). These values were based on the best-fit curve (Equations 1 and 2) to R_S data collected from eight lenses of the same genotype. Loss of 50% AQP0 in AQP0-Htz and TgAQP1/AQP0-Htz caused a significant decrease in resistance and approximately 3-fold increase in radial coupling conductance in the mature fibers (Fig. 4; Table 2). Increased P_f in TgAQP1/AQP0-Htz did not alter GJ coupling resistance or HP compared to AQP0-Htz (Fig. 4; Tables 2, 3).

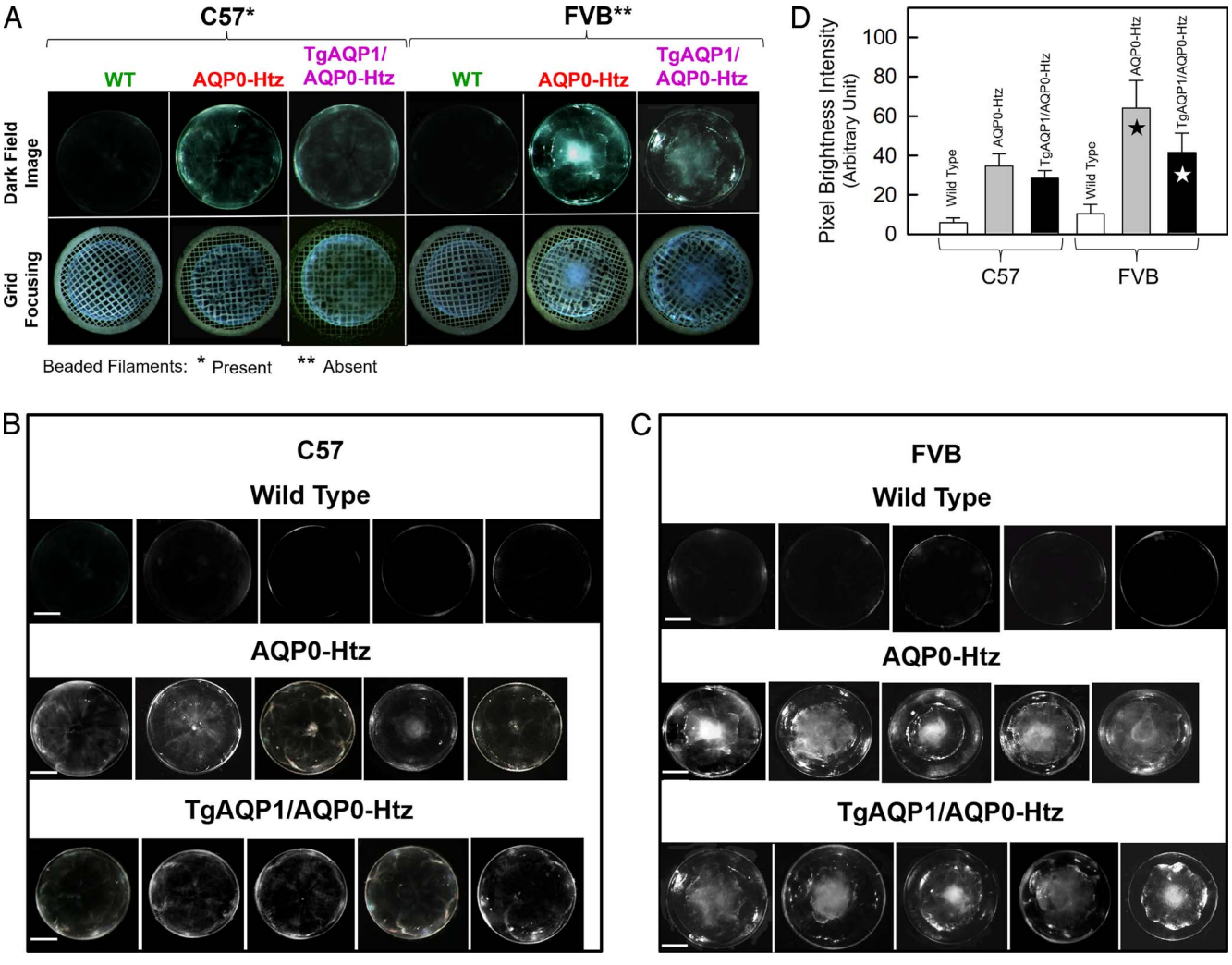

Figure 2. Comparison of two-month-old C57 (with BF) and FVB (without BF) mouse lenses. (**A**) *Top row*: Transparency. WT lenses are transparent except a thin layer of light scattering was observed in the capsule and anterior epithelial cells. AQP0-Htz and TgAQP1/AQP0-Htz lenses from both strains showed light scattering throughout the lens. AQP0-Htz and TgAQP1/AQP0-Htz lenses in FVB suffered more severe cataract than comparable genotype lenses in C57. Lenses were imaged with anterior pole facing up. (**A**) *Bottom row*: Qualitative evaluation of lens spherical aberration: lenses focusing EM metal grid. (**B**) Images showing lens transparency of WT, AQP0-Htz, and TgAQP1/AQP0-Htz mice in C57 genetic background. (**C**) Images showing lens transparency of WT, AQP0-Htz, and TgAQP1/AQP0-Htz mice in FVB genetic background. (**D**) Quantification of lens transparency in WT, AQP0-Htz, and TgAQP1/AQP0-Htz in C57 and FVB mouse strains. *Significant ($P < 0.001$) decrease in lens transparency in FVB than C57.

Investigative Ophthalmology & Visual Science

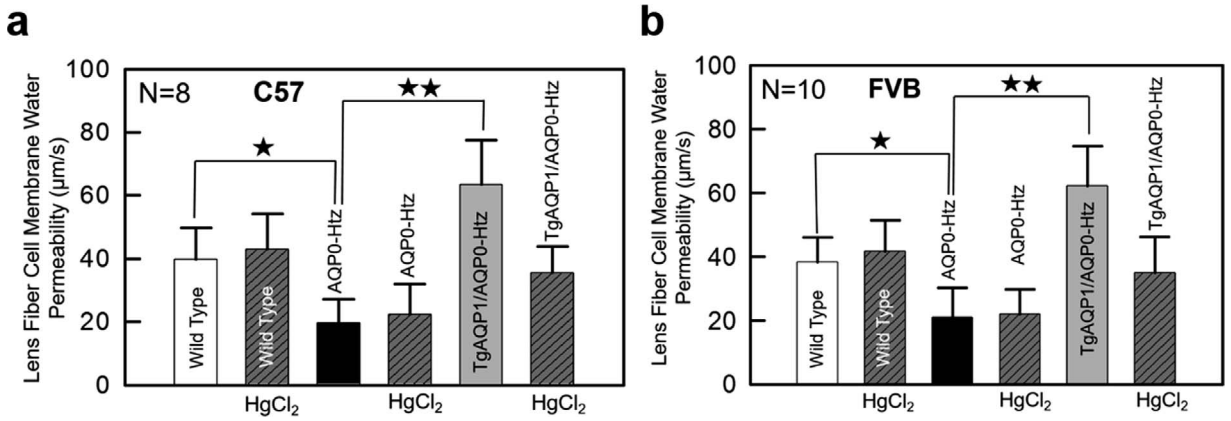

Figure 3. Lens fiber cell membrane P_f of 2-month-old WT, AQP0-Htz, and TgAQP1/AQP0-Htz mice in (**a**) C57 and (**b**) FVB genetic backgrounds. Exposure of fiber cell membrane vesicles to 1 mM $HgCl_2$ was to test for inhibition of P_f. AQP1 is Hg-sensitive whereas AQP0 is not. Each *bar* represents mean ± SD. Eight membrane vesicles were used per experiment. *Significant reduction in P_f in AQP0-Htz compared to WT. **Significant increase in P_f in TgAQP1/AQP0-Htz compared to AQP0-Htz.

In previous studies, the HP at the center of the lens ($p_i[0]$) always varied with the GJ coupling resistance of the central mature fibers. If the resistance went up, pressure went up. In the Cx46 heterozygous KO lenses, the MF resistance doubled and $p_i(0)$ essentially doubled,[36] suggesting no significant change in water flow. Similarly, in Cx46 for Cx50 knockin lenses, the MF resistance was reduced to 50% and $p_i(0)$ was reduced to approximately 50%,[36] again suggesting no significant change in water flow. In the lenses studied here, the data on the radial distribution of intracellular pressure were fit with Equation 3 to determine the pressure at the lens surface ($p_i[a]$) at the transition from DF to MF ($p_i[b]$) and at the lens center ($p_i[0]$; Figs. 4C, 4D, Table 3). $p_i(0)$ decreased in the Htz lenses as expected given the reduced coupling resistance, but the change in $p_i(0)$ was not nearly as great as the change in resistance. The value of R_{MF} decreased nearly 3-fold in the Htz lenses relative to WT, whereas $p_i(0)$ was reduced by 34% to 46% compared to WT. Thus, there may be more water flow in the Htz lenses than WT. Increased P_f in AQP0-Htz (TgAQP1/AQP0-Htz) did not alter the HP compared to AQP0-Htz (Figs. 4C, 4D; Table 3).

Expression of Lens Cx

The increased coupling conductance seen in the C57 Htz lenses suggested there might be an increase in GJ protein expression. Therefore, we looked at expression levels of the major lens Cxs.

Table 1. Lens Fiber Cell Membrane Water Permeability of WT, AQP0-Htz, and TgAQP1/AQP0-Htz Lenses in FVB and C57 Strains

	Fiber Cell Membrane Water Permeability (μm/s)	
	Mouse Strain	
Genotype	C57	FVB
WT	39.75 ± 10.05	38.40 ± 7.66
WT*	43.00 ± 11.24	41.70 ± 9.82
AQP0-Htz	19.63 ± 7.60	21.10 ± 9.17
AQP0-Htz*	22.38 ± 9.64	22.00 ± 7.69
TgAQP1/AQP0-Htz	63.38 ± 14.13	62.30 ± 12.35
TgAQP1/AQP0-Htz*	35.50 ± 8.38	35.00 ± 11.23

* 1mM $HgCl_2$.

Immunoblotting of total lens membrane proteins extracted from WT, AQP0-Htz, and TgAQP1/AQP0-Htz was performed to ascertain whether there were changes in Cx43, Cx46, or Cx50 GJ protein expression levels (Fig. 5A). We tested AQP0-Htz to see the effect when only one copy of AQP0 is expressed. We also tested TgAQP1/AQP0-Htz, which has one copy of AQP0 and transgenically expresses the approximately 40-fold more efficient water channel AQP1[83] in the fiber cells. Equal quantities of the membrane proteins extracted from the different genotypes (in the C57 strain) were tested using anti-Cx43, anti-Cx46, and anti-Cx50 antibodies. Western blotting (Fig. 5A) and protein quantification (Fig. 5B) studies on lens Cx showed no statistically significant difference ($P > 0.05$) in the expression levels of Cx43, 46, or 50 among WT, AQP0-Htz, and TgAQP1-AQP0-Htz lenses. Thus, the increased GJ conductance in C57 AQP0-Htz probably is due to reduction in the abundance of AQP0 causing reorganization of GJs at the membrane in the presence of BF proteins, aided by the gradual post-translational covalent modifications that occur in the proteins involved.

Discussion

A previous study on AQP0-Htz and TgAQP1/AQP0-Htz mouse models developed in FVB background showed no significant alteration in GJ coupling or HP.[30] However, in our study using the same type of mouse models but in the C57 background, which expresses BFs, we found approximately 3-fold reduction in GJ coupling resistance and a 34% to 46% reduction in intracellular HP. Even though AQP1 in the fiber cells of the TgAQP1/AQP0-Htz restored P_f compared to the AQP0-Htz, it did not reduce the HP further, suggesting that HP might be determined by GJ coupling. We see the increase in GJ conductance was not due to an increase in GJ protein expression, though there clearly was an increase in the number of open GJ channels conducting radial ion and water flow. Our data suggested modulation of lens GJ coupling conductance by AQP0 in the presence of BFs.

Loss of BF proteins, CP49, and filensin, in the CP49 KO lens did not cause a significant difference in the expression levels of Cx or GJ coupling conductance.[64,82] Nevertheless, loss of BF proteins and Tropomodulin-1 (Tmod1, actin filament pointed end-capping protein) together resulted in increased GJ resistance and increased HP with no change in Cx expression.[82] The investigators hypothesized that BF and Tmod1 acted like a corral to contain GJ channels on the broad faces of

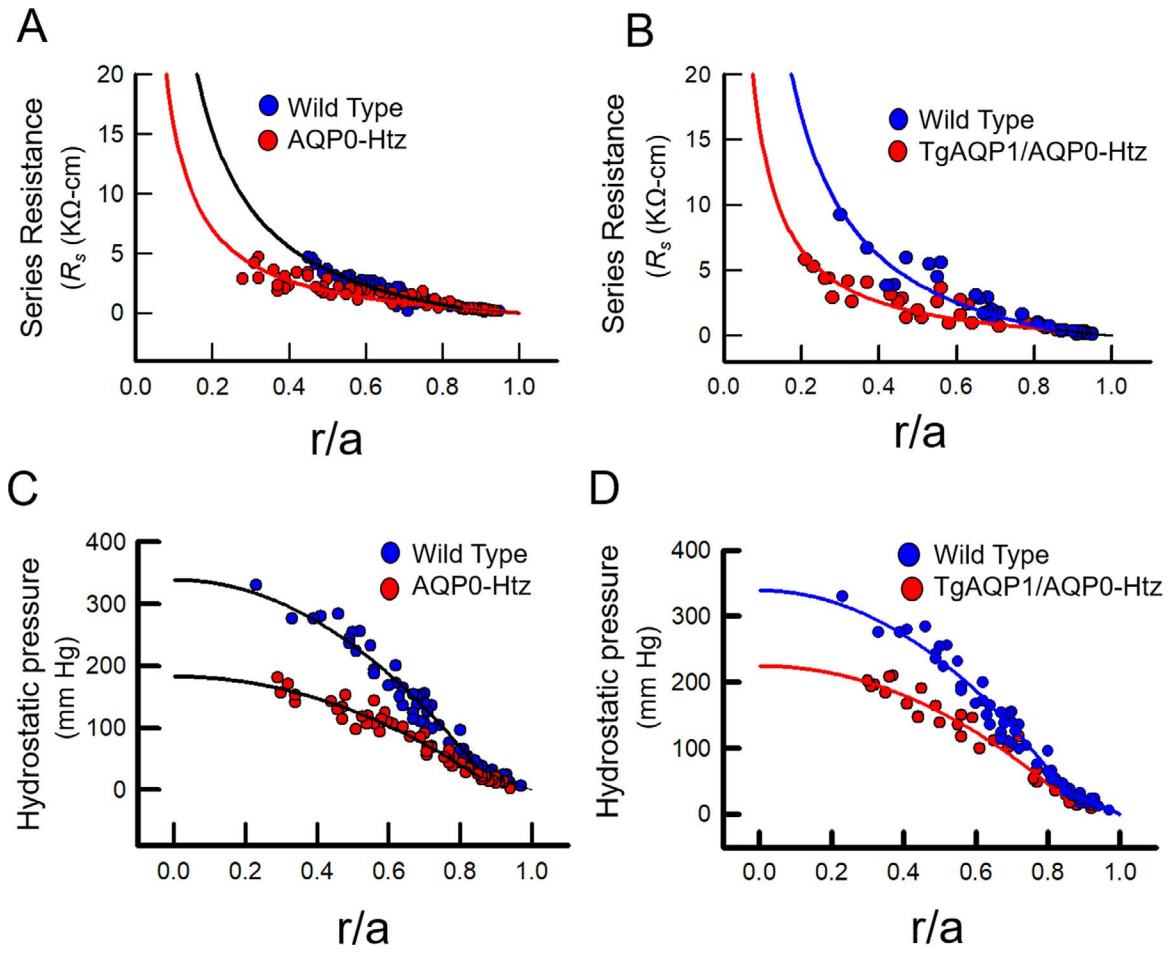

Figure 4. Series resistance and HP in 2-month-old lenses of WT, AQP0-Htz, and TgAQP1/AQP0-Htz mice. (**A**, **B**) Series resistance (R_s) of lenses of: AQP0-Htz ([**A**]; $n = 8$) and TgAQP1/AQP0-Htz ([**B**]; $n = 8$) compared to corresponding data for WT ([**A**, **B**]; $n = 8$), as a function of distance from lens center (r/a), where 'r' (cm) is the actual distance and 'a' (cm) is the lens radius. Lenses of AQP0-Htz and TgAQP1/AQP0-Htz mice showed a significant decrease ($P < 0.001$) in resistance compared to WT. (**C**, **D**) Intracellular HP of lenses of AQP0-Htz ([**C**]; $n = 8$) and TgAQP1/AQP0-Htz ([**D**]; $n = 8$) as a function of normalized distance from lens center (r/a) showed a significant decrease ($P < 0.001$) compared to WT.

Table 2. Regional Values of Resistivity and Normalized Coupling Conductance of WT, AQP0-Htz, and TgAQP1/AQP0-Htz Lenses in C57 Compared to FVB Strain

		Mouse Strain			
		C57	FVB*	C57	FVB*
Genotype	Zone	R_i, KΩ-cm	R_i, KΩ-cm	G_i, S/cm^2	G_i, S/cm^2
WT	DF	3.95	3.60	0.84	0.92
WT	MF	6.19	5.16	0.54	0.65
AQP0-Htz	DF	4.09	3.52	0.81	0.95
AQP0-Htz	MF	2.18	5.44	1.53	0.61
TgAQP1/AQP0-Htz	DF	4.09	4.36†	0.81	0.82†
TgAQP1/AQP0-Htz	MF	2.36	6.26**	1.41	0.53**

R_i, resistivity; G_i, conductance; DF, differentiating fibers; MF, mature fibers.

* Hall and Mathias.[30]

† This study was done at a different time than the comparison of WT with AQP0-Htz, hence they have a different set of control data with WT R_i(DF) = 4.09 and R_i(MF) = 6.03; WT G_i(DF) = 0.81 and G_i(MF) = 0.55.

Table 3. Regional Values of Intracellular HP in WT, AQP0-Htz and TgAQP1/AQP0-Htz Lenses in C57 Compared to FVB Strain

		Mouse Strain	
		C57	FVB*
Genotype	Zone	p_i (mm Hg)	p_i (mm Hg)
WT	p_i(a)	0	0
WT	p_i(b)	35	34
WT	p_i(0)	339	347
AQP0-Htz	p_i(a)	0	0
AQP0-Htz	p_i(b)	22	32
AQP0-Htz	p_i(0)	183	330
TgAQP1/AQP0-Htz	p_i(a)	0	0†
TgAQP1/AQP0-Htz	p_i(b)	23	32†
TgAQP1/AQP0-Htz	p_i(0)	225	332†

p_i(a), pressure at lens surface; p_i(b), pressure at the junction between differentiating fibers and mature fibers; p_i(0), pressure in the center of the lens.

* Hall and Mathias.[30]

† This study was done at a different time than the comparison of WT with AQP0-Htz, hence they have a different set of control data with WT p_i(a) = 0, p_i(b) = 35; p_i(0) = 339.

Investigative Ophthalmology & Visual Science

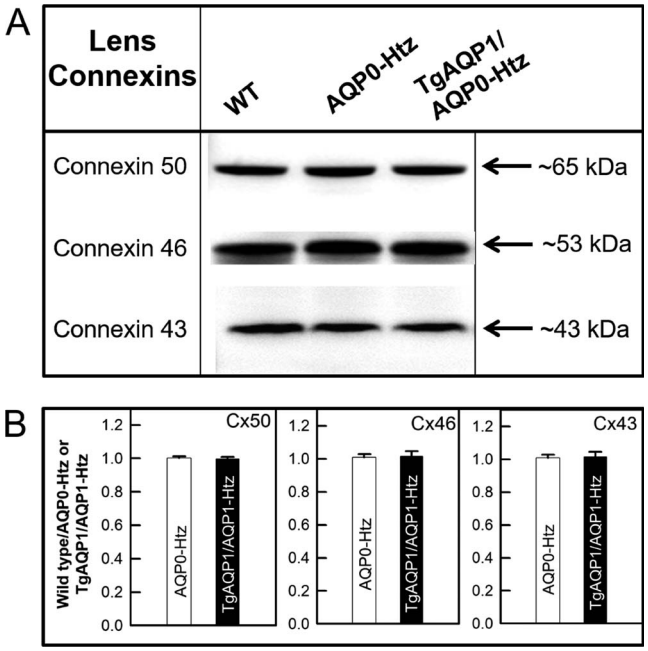

Figure 5. Western blotting to assess the expression levels of Cx50, Cx46, and Cx43 in the WT, AQP0-Htz and TgAQP1/AQP0-Htz lenses in C57 background. (**A**) Cx50, Cx46, and Cx43 polypeptides recognized by their respective antibodies. *Arrows* show the relative molecular size as indicated for the respective Cx. (**B**) Quantification and comparison of protein expression levels of Cx50, Cx46, and Cx43 in the lenses of AQP0-Htz and TgAQP1/AQP0-Htz with those of WT. The protein quantification data shown for the different Cxs represent mean ± SD of four or five independent Western blot analyses using 2-month-old mice lenses from different litters.

fiber cells. Loss of both resulted in smaller and more dispersed GJ plaques in the broad faces of fiber cells as well as increased GJ resistance and HP. Perhaps the opposite happens in the AQP0-Htz lenses of C57 background that expresses BFs. In C57 AQP0-Htz, lack of 50% of AQP0 protein in the broader side of the fiber cells might be facilitating the small GJ plaques to form large ones in the presence of BF proteins to enable more efficient GJ coupling in the radial direction. Increased GJ coupling, consequently, could be creating a more efficient microcirculation to maintain lens homeostasis and reduce cataract severity in C57 AQP0-Htz lenses. AQP0-Htz lenses in FVB genetic background, that does not express BFs, develop severe cataract likely due to failure of small GJ junction plaques in the narrow sides of the fiber cells to migrate to the broader sides for increased GJ coupling and efficient microcirculation.

In the current study, increase in GJ coupling and reduction in HP are due to regulation of GJs by AQP0 in the presence of BF proteins, rather than indirect effects of the genetic manipulation causing membrane reorganization as a consequence of the loss of 50% of the profusely expressed AQP0. In the differentiating fiber cells of the WT lens, AQP0 and GJs are distributed more or less uniformly (with respect to their expression levels in the lens) throughout the membrane except at some specific regions of the fiber cell membranes. In the maturing fiber cells, AQP0 forms thin junctional square arrays and drives the GJs to its periphery.[88,91] In AQP0-Htz, reduction of AQP0 protein by 50% altered GJ localization and function. Electron microscopy (EM) studies by Al-Ghoul et al.[50] and atomic force microscopy studies by Buzhynskyy et al.[88] and Scheuring et al.[91] are relevant to our notion. When another abundantly expressed (approximately 11% of the total fiber cell membrane proteins[95]) lens membrane protein MP20 (Lim2) was deleted by 50% or 100%, there was no increase in GJ coupling due to clearing of membrane space and the subsequent membrane remodeling; rather there was a decrease in GJ coupling and the lenses were normal and transparent.[81] KO of BF protein CP49 did not alter the GJ coupling.[64,82] Our data implied that in the presence of BF proteins, AQP0 reduces GJ coupling in WT lenses during the fiber cell maturation process by driving the GJs to the periphery of its thin junctional square arrays, since there is gradual reduction in metabolic activity in the maturing fiber cells.

Determinants of fiber cell architecture, such as MP20,[81] AQP0, and BFs, appear to be involved in the regulation of GJ coupling in the lens. A previous investigation on lens fiber membranes of an AQP0-Htz in a mixed strain revealed that the percentage of GJ area remained basically the same as in WT while the mean area/GJ increased significantly in AQP0-Htz mouse lenses.[50] The study reported that AQP0 square array junctions were seen readily in WT but were absent in the AQP0-Htz. However, no data are available on GJ coupling or HP and expression of BF proteins in this mixed genetic background AQP0-Htz for comparison with our current data.

The Effect of GJ Coupling on the Lens Circulation and HP

Homeostasis in the avascular lens requires a microcirculation facilitated by AQPs, GJ channel, and ion channels. During the intracellular phase of the microcirculation, Na^+ passes from the central fibers to the surface cells through GJ channels. As sodium enters fiber cells and flows to the surface, transmembrane osmotic gradients are generated and water enters the fiber cells through AQP0 and follows the flow of Na^+ to the surface. To drive the cell-to-cell flow of sodium, there are intracellular diffusion and voltage gradients and to drive cell-to-cell water flow, there is an intracellular HP gradient.[36] With a rise in GJ coupling, there is a decrease in the intracellular gradients for voltage, sodium diffusion, and HP.[36,84] We documented a decrease in the HP gradient with the increase in open GJ channels; however, the pressure gradient did not go down as much as the coupling resistance. The HP gradient is dictated by water flow, which follows transmembrane sodium inflow. The reduction in GJ resistance will make the intracellular voltage more negative and reduce sodium radial-diffusion gradients. These changes could increase transmembrane sodium inflow and, thus, increase water flow. These simple indirect effects of reduced GJ resistance could lead to increased water flow, but the AQP0-Htz effect on water flow remains uncertain.

AQP0 Water Permeability Effect on Lens Water Flow and HP

Hall and Mathias[30] provide an extensive discussion of the effect of membrane water permeability on water flow. The essence of their conclusions and data are that membrane P_f is much larger than salt permeability, so salt transport is rate-limiting for osmosis. Increasing fiber cell membrane P_f would not significantly increase water flow, which already is near maximal. Moreover, there would need to be a huge reduction in membrane P_f to significantly reduce water flow and, thus, reduce HP. They show that in FVB mice, expression of transgenic AQP1 (TgAQP1/AQP0-Htz) more than doubles fiber cell membrane P_f without appreciably affecting water flow or HP, and that in AQP0-Htz mice, fiber cell membrane P_f is reduced to approximately half that of WT mice without appreciably affecting water flow or HP. They also report no change in GJ coupling conductance in AQP0-Htz, FVB mice,

Investigative Ophthalmology & Visual Science

whereas here we reported a significant increase in GJ coupling conductance in AQP0-Htz, C57 mice. This increase in GJ coupling causes the decrease in HP in AQP0-Htz, C57 mice. GJs provide the path for intracellular outflow of water,[36] so when the number of open GJ channels increases, the resistance for fluid outflow decreases and less pressure is required to drive the same water flow.

Possible Interactions Among AQP0, BFs, and GJs

In our study, loss of 50% of AQP0 caused a significant decrease in GJ coupling resistance and lens HP in the MF region, probably through effects on Cx46 rather than Cx50 GJs, since Cx46 is thought to be the only functional MF channel.[15,16,67,78,79,85] Modulation of Cx46 by AQP0 could be direct. One such effect simply could be the abundance of AQP0 protein in the membrane; also, AQP0 forms large square arrays of thin junctions (11–13 nm) in the maturing fiber cells of MF region.[86,87] AQP0 thin junctions in this region appear to push the GJ plaques (16–17 nm) toward the periphery of the thin junctional square arrays.[88–92] The observed increase in lens GJ coupling could be due to the increased availability of membrane space on the fiber cells' broad surfaces, which mediate radial flows. If GJs were corralled by BFs in the broad faces,[82] we would record a reduction in the radial GJ resistance as area normally filled with square arrays is filled with large GJ plaques. Thus, the increase in GJ coupling possibly could be caused by GJ channel plaque reorganization and distribution, which will be analyzed in the future using ultrastructural studies.

C-Terminal Truncation of AQP0 and Lens Cx

At the DF to MF transition, which occurs at approximately 15% of the distance into a mouse lens or 85% of the distance from the lens center, organelles are degraded and most membrane and cytosolic proteins begin to undergo PTMs (e.g., C-terminal truncation). C-terminal truncation of AQP0 does not appear to alter its water permeability,[2,93] though it may induce formation of thin junctions, which are much more prevalent in the MF (inner cortex and outer nuclear regions) than DF.[2,94] A number of studies (reviewed by Mathias et al.[16]) suggest C-terminal truncation of Cx50 at the DF to MF transition causes the open probability of Cx50 channels to drop to near zero, so coupling conductance decreases, as seen for WT lenses in Table 2. C-terminal truncation of Cx46 does not affect the conductance of Cx46 channels, so coupling of MF region is thought almost exclusively to be due to Cx46 channels. Also, as seen in Table 2, expression of AQP0-Htz in lenses from C57 mice causes the Cx46 channels in the MF region to increase coupling conductance relative to those in DF region. There is no significant change in GJ coupling of the DF in AQP0-Htz lenses relative to WT. There also is no significant change in GJ coupling of either the DF or MF region in AQP0-Htz lenses from FVB mice, which lack BFs. Together, these studies suggest modulation of Cx46 GJ coupling conductance by AQP0 in the maturing fiber cells of the MF region, in the presence of BF proteins in the lens.

From our results, we hypothesized that the AQP0 tetramer square array density in the maturing fiber cells of inner cortex and outer nucleus could modulate lens GJ function for normal lens microcirculation to maintain lens transparency and homeostasis. Our hypothesis is depicted as models for WT and AQP0-Htz in Figures 6A and 6B. Due to the similarities in results for C57 TgAQP1/AQP0-Htz with AQP0-Htz, we did not attempt to provide a separate model for the former. The models are designed to represent the four putative regions of the lens, namely outer cortex, inner cortex, outer nucleus, and inner nucleus, because AQP0 and several other lens membrane and cytosolic proteins undergo gradual N- and C-terminal end cleavages, from the inner cortex to the inner nucleus.

In the WT (Fig. 6A, left column), intact AQP0 present at the outer cortex interacts with cytoskeletal proteins (e.g., BF proteins)[46,47] and GJ proteins (Cx),[17] possibly aiding in the relatively uniform distribution of AQP0 in the fiber cell membranes.[2] AQP0 constitutes approximately 45% of the total membrane proteins;[95] it interacts with Cx, BF proteins, and crystallins through the C-terminus.[2,96] During fiber cell maturation from inner cortex to outer nucleus, AQP0, Cx, and several other lens proteins undergo gradual deletion of N- and C-terminal ends, possibly resulting in the gradual loss of protein–protein interactions.[2] This process could be triggering tetrameric AQP0 to group and form small square array thin junctions to provide strong adhesion, and in the process, be pushing the interspersed GJs to the periphery. The presence of GJ plaques at the periphery of AQP0 square array thin junctions has been reported by Buzhynskyy et al.[88,89] As the distance to the lens interior advances, formation of more AQP0 large square array thin junctions occur in the nucleus, possibly to ensure tight holding of the fiber cells to reduce the extracellular space and aid in the compact packing of the maturing and matured fibers. The GJ plaques may reach a medium size into the lens but do not attain large sizes probably due to the abundant expression of AQP0 and presence of large AQP0 square array thin junctions.

In the AQP0-Htz (Fig 6A, right column) outer cortex, intact AQP0 may follow the same distribution in principle as in the WT, but with only 50% AQP0 present, there is more space in the membrane. During fiber cell maturation in the inner cortex, outer nucleus, and inner nucleus, availability of more membrane space possibly allows the GJs to move and form large plaques and more open channels; this could be the reason for the increased GJ conductance in AQP0-Htz. Higher GJ coupling conductance has been reported for larger compared to smaller plaques.[82] The increase in GJ conductance might have facilitated a decrease in HP. However, even the increase in GJ conductance and decrease in HP were not enough to restore complete lens transparency and homoeostasis, possibly due to the reduction in cell-to-cell adhesion, which could be a consequence of the lack of 50% AQP0.

A portion of a fiber cell membrane surface representing only AQP0 and GJ proteins is modeled in Figure 6B for WT (top row) and AQP0-Htz (bottom row) lenses in C57 background. At the outer cortex differentiating fibers of the WT, AQP0 tetramers and GJs are distributed throughout the membrane. In the maturing fiber cells at the inner cortex, grouping of AQP0 tetramers and formation of small AQP0 square array thin junctions occur; enrichment of small GJ plaques also occurs, possibly due to the gradual loss of N- and C-terminal ends of lens proteins causing rearrangement of proteins at the membrane surface.[2] This process results in the formation of more and more AQP0 square array thin junctions and GJ plaques from the outer to the inner nucleus, the largest of both being present at the inner nucleus. In AQP0-Htz (Fig. 6B, bottom row), reduction in 50% of AQP0 provides more free space, and post-translational N- and C-terminal end cleavages of proteins allow movement of AQP0 to form collective square array thin junctions, and the GJs to form much larger plaques with more conductance. Formation of large GJ plaques could increase radial GJ coupling and reduce HP.

FVB WT lenses that lack BFs are as transparent as those of C57 WT mice. However, the severe lens cataract phenotype in FVB AQP0-Htz compared to C57 AQP0-Htz could be due to the absence of BFs causing loss of interactions with AQP0 and/or other proteins. The less severe lens cataract phenotype in the

Investigative Ophthalmology & Visual Science

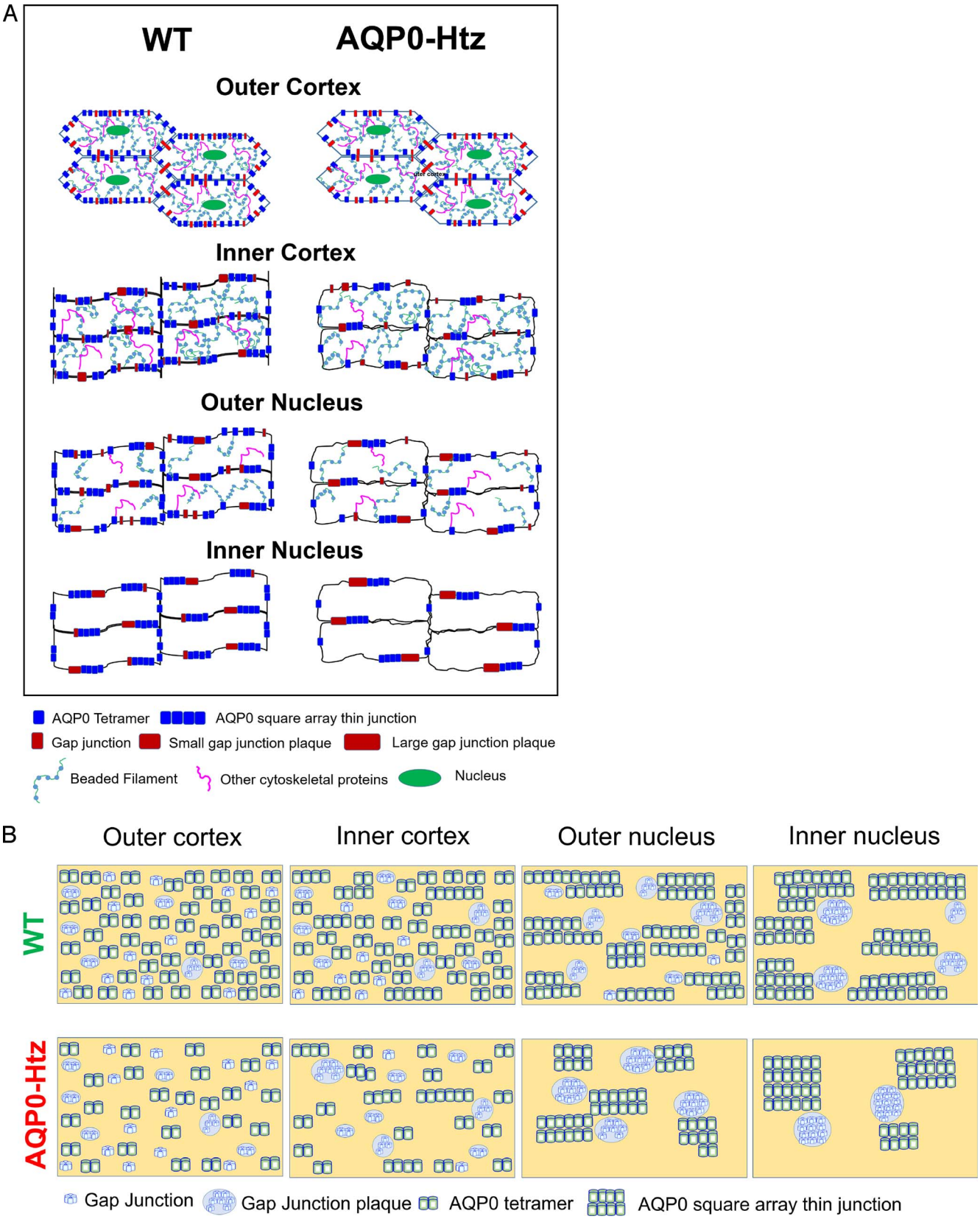

Figure 6. (**A**) Schematic model describing the possible regulation of lens GJ channel distribution and function by AQP0, in WT and AQP0-Htz C57 mouse lens fiber cells. Cross-sectional views of fiber cells at outer cortex, inner cortex, outer nucleus, and inner nucleus are presented. WT (*left column*) lens fiber cells show BFs, AQP0, and GJ plaques and other cytoskeletal proteins in the outer cortex. AQP0 is distributed at the membrane interspersed with GJs. As fiber cells mature (inner cortex and outer nucleus), the cell nucleus is lost, and BFs, AQP0, GJ-, and other proteins begin to lose their N- and C-terminal ends; reorganization of the cell membrane proteins occur. AQP0 group to form larger square array thin junctions and the small GJ plaques are pushed to the periphery of the square arrays. GJs probably are prevented from forming very large plaques due to the prolific

Investigative Ophthalmology & Visual Science

expression of AQP0 and thin junctions. At the inner nucleus in the terminally differentiated fiber cells large patches of square array thin junctions and small to medium GJ plaques are seen. AQP0-Htz (*right column*) mouse lens fiber cells express BFs, 50% AQP0, and 100% Cx and other proteins. The outer cortex may follow the same type of distribution of the proteins but with only 50% of AQP0, which clears more membrane space. Cx GJ channels form larger aggregates of junctional plaques due to the availability of more surface area as a result of the reduction in AQP0 and consequent possible reduction in large patches of AQP0 square array thin junctions. The differentiated fiber cells at the inner nucleus have AQP0 large square array thin junctions and large Cx GJ plaques. Compared to small GJ plaques, large GJ plaques have higher conductance.[82] (**B**) Schematic representations of only AQP0 and GJs at fiber cell membrane surfaces of WT and AQP0-Htz C57 mice lenses. WT (*top row*) outer cortex shows AQP0 tetramers, and Cx distributed optimally. Formation of more GJ plaques, grouping of AQP0, and thin junction formation occur at the inner cortex and outer nucleus probably due to the gradual loss of N- and C-terminal ends of the proteins. These events happen to a greater extent at the inner nucleus and increase in GJ plaque size and AQP0 square array thin junctions occur. AQP0-Htz (*bottom row*) has fewer tetramers compared to the WT with more free space due to the loss of 50% AQP0. Availability of more surface area probably stimulates the smaller GJ plaques to move and aggregate to form larger plaques in the inner cortex, outer nucleus, and inner nucleus. The large GJ plaques with increased GJ coupling might be responsible for the decrease in HP in the AQP0-Htz condition.

AQP0-Htz in C57 mouse strain compared to the cataract phenotype in FVB could be due to the increased efficiency in the lens microcirculation.

Conclusions

In the presence of BF proteins, AQP0 plays a significant role in modulating lens GJ coupling and HP to regulate the microcirculation. Our data are consistent with the hypothesis that the improved transparency in C57 AQP0-Htz lenses is due to modulation of GJ coupling by AQP0 in the presence of BF proteins to increase the circulation of fluid in the lens and support homeostasis. To our knowledge, this is the first report on an aquaporin water channel regulating gap junctions in the lens.

Acknowledgments

The authors thank Alan Shiels, PhD, for providing the original AQP0 knockout mouse model in a mixed background and Paul G. FitzGerald, PhD, for providing antibodies for BF proteins CP49 and CP115.

Supported by funding from National Institute of Health-NEI, Grants R01: EY020506, EY026155 (KV), and R01: EY06391 (RTM).

Disclosure: **S. Kumari**, None; **J. Gao**, None; **R.T. Mathias**, None; **X. Sun**, None; **A. Eswaramoorthy**, None; **N. Browne**, None; **N. Zhang**, None; **K. Varadaraj**, None

References

1. Ball LE, Garland DL, Crouch RK, Schey KL. Post-translational modifications of aquaporin 0 (AQP0) in the normal human lens: spatial and temporal occurrence. *Biochemistry*. 2004; 43:9856–9865.
2. Kumari SS, Varadaraj K. Intact and N- or C-terminal end truncated AQP0 function as open water channels and cell-to-cell adhesion proteins: end truncation could be a prelude for adjusting the refractive index of the lens to prevent spherical aberration. *Biochim Biophys Acta*. 2014;1840:2862–2877.
3. Shiels A, Hejtmancik JF. Mutations and mechanisms in congenital and age-related cataracts. *Exp Eye Res*. 2017;156: 95–102.
4. Bassnett S, Šikić H. The lens growth process. *Prog Retin Eye Res*. 2017;60:181–200
5. Lin JS, Fitzgerald S, Dong YM, Knight C, Donaldson P, Kistler J. Processing of the gap junction protein connexin50 in the ocular lens is accomplished by calpain. *Eur J Cell Biol*. 1997; 73:141–149.
6. Lin JS, Eckert R, Kistler J, Donaldson P. Spatial differences in gap junction gating in the lens are a consequence of connexin cleavage, *Eur J Cell Biol*. 1998;76:246–250.
7. DeRosa AM, Mui R, Srinivas M, White TW. Functional characterization of a naturally occurring Cx50 truncation. *Invest Ophthalmol Vis Sci*. 2006;47:4474–4481.
8. Slavi N, Wang Z, Harvey L, Schey KL, Srinivas M. Identification and functional assessment of age-dependent truncations to Cx46 and Cx50 in the human Lens. *Invest Ophthalmol Vis Sci*. 2016;57:5714–5722.
9. Bassnett S. Lens organelle degradation. *Exp Eye Res*. 2002;74: 1–6.
10. Bassnett S. On the mechanism of organelle degradation in the vertebrate lens. *Exp Eye Res*. 2009;88:133–139.
11. Kumari SS, Varadaraj K. Aquaporin 0 plays a pivotal role in refractive index gradient development in mammalian eye lens to prevent spherical aberration. *Biochem Biophys Res Commun*. 2014;45:986–991.
12. Pierscionek B, Bahrami M, Hoshino M, Uesugi K, Regini J, Yagi N. The eye lens: age-related trends and individual variations in refractive index and shape parameters. *Oncotarget*. 2015;6: 30532–30544.
13. Kumari SS, Gupta N, Shiels A, et al. Role of Aquaporin 0 in lens biomechanics. *Biochem Biophys Res Commun*. 2015; 462:339–345.
14. Mathias RT, Rae JL, Baldo GJ. Physiological properties of the normal lens. *Physiol Rev*. 1997;77:21–50.
15. Mathias RT, Kistler J, Donaldson P. The lens circulation. *J Membr Biol*. 2007;216:1–16.
16. Mathias RT, White TW, Gong X. Lens gap junctions in growth, differentiation, and homeostasis. *Physiol Rev*. 2010;90:179–206.
17. Yu XS, Jiang JX. Interaction of major intrinsic protein (aquaporin-0) with fiber connexins in lens development, *J Cell Sci*. 2004;117:871–880.
18. Beyer EC, Ebihara L, Berthoud VM. Connexin mutants and cataracts. *Front Pharmacol*. 2013;4:43.
19. Beyer EC, Berthoud VM. Connexin hemichannels in the lens. *Front Physiol*. 2014;5:20.
20. Berthoud VM, Minogue PJ, Osmolak P, Snabb JI, Beyer EC. Roles and regulation of lens epithelial cell connexins. *FEBS Lett*. 2014;588:1297–1303.
21. Bevans CG, Kordel M, Rhee SK, Harris AL. Isoform composition of connexin channels determines selectivity among second messengers and uncharged molecules. *J Biol Chem*. 1998;273:2808–2816.
22. Harris AL. Connexin channel permeability to cytoplasmic molecules. *Prog Biophys Mol Biol*. 2007;94:120–143.
23. Gong X, Li E, Klier G, et al. Disruption of alpha3-connexin gene leads to proteolysis and cataractogenesis in mice. *Cell*. 1997;91:833–843.
24. White TW, Goodenough DA, Paul DL. Targeted ablation of connexin50 in mice results in microphthalmia and zonular pulverulent cataracts. *J Cell Biol*. 1998;143:815–825.

25. Varadaraj K, Kushmerick C, Baldo GJ, et al. The role of MIP in lens fiber cell membrane transport. *J Membr Biol*. 1999;170: 191–203.
26. Varadaraj K, Kumari S, Mathias T. Transgenic expression of AQP1 in the fiber cells of AQP0 knockout mouse: effects on lens transparency. *Exp Eye Res*. 2010;91:393–404.
27. Shiels A, Bassnett S, Varadaraj K, et al. Optical dysfunction of the crystalline lens in aquaporin-0-deficient mice. *Physiol Genomics*. 2001;7:179–186.
28. Kumari SS, Eswaramoorthy S, Mathias RT, Varadaraj K. Unique and analogous functions of aquaporin 0 for fiber cell architecture and ocular lens transparency. *Biochim Biophys Acta*. 2011;1812:1089–1097.
29. Kumari SS, Gandhi J, Mustehsan MH, Eren S, Varadaraj K. Functional characterization of an AQP0 missense mutation, R33C, that causes dominant congenital lens cataract, reveals impaired cell-to-cell adhesion. *Exp Eye Res*. 2013;116:371–385.
30. Hall JE, Mathias RT. The aquaporin zero puzzle. *Biophys J*. 2014;107:10–15.
31. Donaldson P, Kistler J, Mathias RT. Molecular solutions to mammalian lens transparency. *News Physiol Sci*. 2001;16: 118–123.
32. Donaldson PJ, Grey AC, Maceo Heilman B, Lim JC, Vaghefi E. The physiological optics of the lens. *Prog Retin Eye Res*. 2017;56:e1–e24.
33. Kumari SS, Varadaraj K. Aquaporin 5 knockout mouse lens develops hyperglycemic cataract. *Biochem Biophys Res Commun*. 2013;441:333–338.
34. Grey AC, Walker KL, Petrova RS, et al. Verification and spatial localization of aquaporin-5 in the ocular lens. *Exp Eye Res*. 2013;108:94–102.
35. Gao J, Sun X, Yatsula V, Wymore RS, Mathias RT. Isoform-specific function and distribution of Na/K pumps in the frog lens epithelium. *J Membr Biol*. 2000;178:89–101.
36. Gao J, Sun X, Moore LC, White TW, Brink PR, Mathias RT. Lens intracellular hydrostatic pressure is generated by the circulation of sodium and modulated by gap junction coupling. *J Gen Physiol*. 2011;137:507–520.
37. Candia OA, Mathias R, Gerometta R. Fluid circulation determined in the isolated bovine lens. *Invest Ophthalmol Vis Sci*. 2012;53:7087–7096.
38. Vaghefi E, Pontre BP, Jacobs MD, Donaldson PJ. Visualizing ocular lens fluid dynamics using MRI: manipulation of steady state water content and water fluxes. *Am J Physiol Regul Integr Comp Physiol*. 2011;301:R335–342.
39. Mathias RT, Riquelme G, Rae JL. Cell to cell communication and pH in the frog lens. *J Gen Physiol*. 1991;98:1085–1103.
40. Bassnett S, Croghan PC, Duncan G. Diffusion of lactate and its role in determining intracellular pH in the lens of the eye. *Exp Eye Res*. 1987;44:143–147.
41. Yorio T, Cruz E, Bentley PJ. Aerobic and anaerobic metabolism of the crystalline lens of a poikilotherm; the toad *Bufo marinus*. *Comp Biochem Physiol B*. 1979;62:123–126.
42. Schey KL, Wang Z, Wenke JL, Qi Y. Aquaporins in the eye: expression, function, and roles in ocular disease. *Biochim Biophys Acta*. 2014;1840:1513–1523.
43. Liu J, Xu J, Gu S, Nicholson BJ, Jiang JX. Aquaporin 0 enhances gap junction coupling via its cell adhesion function and interaction with connexin 50. *J Cell Sci*. 2011;124:198–206.
44. Yu XS, Yin X, Lafer EM, Jiang JX. Developmental regulation of the direct interaction between the intracellular loop of connexin 45.6 and the C terminus of major intrinsic protein (aquaporin-0). *J Biol Chem*. 2005;280:22081–22090.
45. Dunia I, Recouvreur M, Nicolas P, Kumar N, Bloemendal H, Benedetti EL. Assembly of connexins and MP26 in lens fiber plasma membranes studied by SDS-fracture immunolabeling. *J Cell Sci*. 1998;111:2109–2120.
46. Lindsey Rose KM, Gourdie RG, Prescott AR, Quinlan RA, Crouch RK, Schey KL. The C terminus of lens aquaporin 0 interacts with the cytoskeletal proteins filensin and CP49. *Invest Ophthalmol Vis Sci*. 2006;47:1562–1570.
47. Wang Z, Schey KL. Identification of a direct Aquaporin-0 binding site in the lens-specific cytoskeletal protein filensin. *Exp Eye Res*. 2017;159:23–29.
48. Shiels A, Bassnett S. Mutations in the founder of the MIP gene family underlie cataract development in the mouse. *Nat Gen*. 1996;12:212–215.
49. Shiels A, Mackay D, Bassnett S, Al-Ghoul K, Kuszak J. Disruption of lens fiber cell architecture in mice expressing a chimeric AQP0-LTR protein. *FASEB J*. 2000;14:2207–2212.
50. Al-Ghoul KJ, Kirk T, Kuszak AJ, Zoltoski RK, Shiels A, Kuszak JR. Lens structure in MIP-deficient mice. *Anat Rec A Discov Mol Cell Evol Biol*. 2003;273:714–730.
51. Okamura T, Miyoshi I, Takahashi K, et al. Bilateral congenital cataracts result from a gain-of-function mutation in the gene for aquaporin-0 in mice. *Genomics*. 2003;81:361–368.
52. Bennett TM, Zhou Y, Shiels A. Lens transcriptome profile during cataract development in Mip-null mice. *Biochem Biophys Res Commun*. 2016;478:988–993.
53. Zhou Y, Bennett TM, Shiels A. Lens ER-stress response during cataract development in Mip-mutant mice. *Biochim Biophys Acta*. 2016;1862:1433–1442.
54. Francis P, Berry V, Bhattacharya S, Moore A. Congenital progressive polymorphic cataract caused by a mutation in the major intrinsic protein of the lens, MIP (AQP0). *Br J Ophthalmol*. 2000;84:1376–1379.
55. Song Z, Wang L, Liu Y, Xiao W. A novel nonsense mutation in the MIP gene linked to congenital posterior polar cataracts in a Chinese family. *PLoS One*. 2015;10:e0119296.
56. Mulders SM, Preston GM, Deen PM, Guggino WB, van Os CH, Agre P. Water channel properties of major intrinsic protein of lens. *J Biol Chem*. 1995;270:9010–9016.
57. Kushmerick C, Rice SJ, Baldo GJ, Haspel HC, Mathias RT. Ion, water and neutral solute transport in *Xenopus* oocytes expressing frog lens MIP. *Exp Eye Res*. 1995;61:351–362.
58. Zampighi GA, Kreman M, Boorer KJ, et al. A method for determining the unitary functional capacity of cloned channels and transporters expressed in *Xenopus laevis* oocytes. *J Membr Biol*. 1995;148:65–78.
59. Michea LF, de la Fuente M, Lagos N. Lens major intrinsic protein (MIP) promotes adhesion when reconstituted into large unilamellar liposomes. *Biochemistry*. 1994;33:7663–7669.
60. Michea LF, Andrinolo D, Ceppi H, Lagos N. Biochemical evidence for adhesion-promoting role of major intrinsic protein isolated from both normal and cataractous human lenses. *Exp Eye Res*. 1995;61:293–301.
61. Kumari SS, Varadaraj K. Intact AQP0 performs cell–to-cell adhesion. *Biochem Biophys Res Commun*. 2009;390:1034–1039.
62. Lo WK, Biswas SK, Brako L, Shiels A, Gu S, Jiang JX. Aquaporin- targets interlocking domains to control the integrity and transparency of the eyelens. *Invest Ophthalmol Vis Sci*. 2014;55:1202–1212.
63. Biswas SK, Brako L, Gu S, Jiang JX, Lo WK. Regional changes of AQP0-dependent square array junction and gap junction associated with cortical cataract formation in the Emory mutant mouse. *Exp Eye Res*. 2014;127:132–142.
64. Fudge DS, McCuaig JV, Van Stralen S, et al. Intermediate filaments regulate tissue size and stiffness in the murine lens. *Invest Ophthalmol Vis Sci*. 2011;52:3860–3867.

Investigative Ophthalmology & Visual Science

65. Gokhin DS, Nowak RB, Kim NE, et al. Tmod1 and CP49 synergize to control the fiber cell geometry, transparency, and mechanical stiffness of the mouse lens. *PLoS One*. 2012;7: e48734.
66. Varadaraj K, Kumari SS, Patil R, Wax MB, Mathias RT. Functional characterization of a human aquaporin 0 mutation that leads to a congenital dominant lens cataract. *Exp Eye Res*. 2008;87:9–21.
67. Gao J, Sun X, Martinez-Wittinghan FJ, Gong X, White TW, Mathias RT. Connections between connexins, calcium, and cataracts in the lens. *J Gen Physiol*. 2004;124:289–300.
68. Gong X, Agopian K, Kumar NM, Gilula NB. Genetic factors influence cataract formation in alpha 3 connexin knockout mice. *Dev Genet*. 1999;24:27–32.
69. Gerido DA, Sellitto C, Li L, White TW. Genetic background influences cataractogenesis, but not lens growth deficiency, in Cx50-knockout mice. *Invest Ophthalmol Vis Sci*. 2003;44: 2669–2674.
70. Simirskii VN, Lee RS, Wawrousek EF, Duncan MK. Inbred FVB/ N mice are mutant at the cp49/Bfsp2 locus and lack beaded filament proteins in the lens. *Invest Ophthalmol Vis Sci*. 2006;47:4931–4934.
71. Alizadeh A, Clark J, Seeberger T, Hess J, Blankenship T, FitzGerald PG. Characterization of a mutation in the lens-specific CP49 in the 129 strain of mouse. *Invest Ophthalmol Vis Sci*. 2004;45:884–891.
72. Varadaraj K, Kumari SS, Mathias RT. Functional expression of aquaporins in embryonic, postnatal, and adult mouse lenses. *Dev Dyn*. 2007;236:1319–1328.
73. Kumari SS, Varadaraj M, Yerramilli VS, Menon AG, Varadaraj K. Spatial expression of aquaporin 5 in mammalian cornea and lens and regulation of its localization by phosphokinase A. *Mol Vis*. 2012;18:957–967.
74. Varadaraj K, Kumari S, Shiels A, Mathias RT. 2005. Regulation of aquaporin water permeability in the lens. *Invest Ophthalmol Vis Sci*. 2005;46:1393–1402.
75. Sandilands A, Wang X, Hutcheson AM, et al. Bfsp2 mutation found in mouse 129 strains causes the loss of CP49′ and induces vimentin-dependent changes in the lens fiber cell cytoskeleton. *Exp Eye Res*. 2004;78:875–889.
76. Preston GM, Carroll TP, Guggino WB, Agre P. Appearance of water channels in *Xenopus* oocytes expressing red cell CHIP28 protein. *Science*. 1992;256:385–387.
77. Agre P, Preston GM, Smith BL, et al. Aquaporin CHIP: the archetypal molecular water channel. *Am J Physiol*. 1993;265: 463–476.
78. Gong X, Baldo GJ, Kumar NM, Gilula NB, Mathias RT. Gap junctional coupling in lenses lacking alpha3 connexin. *Proc Natl Acad Sci U S A*. 1998;95:15303–15308.
79. Baldo GJ, Gong X, Martinez-Wittinghan FJ, Kumar NM, Gilula NB, Mathias RT. Gap junctional coupling in lenses from alpha(8) connexin knockout mice. *J Gen Physiol*. 2001;118: 447–456.
80. Martinez-Wittinghan FJ, Sellitto C, White TW, Mathias RT, Paul D, Goodenough DA. Lens gap junctional coupling is modulated by connexin identity and the locus of gene expression. *Invest Ophthalmol Vis Sci*. 2004;45:3629–3637.
81. Shi Y, De Maria AB, Wang H, Mathias RT, FitzGerald PG, Bassnett S. Further analysis of the lens phenotype in Lim2-deficient mice. *Invest Ophthalmol Vis Sci*. 2011;52:7332–7339.
82. Cheng C, Nowak RB, Gao J, et al. Lens ion homeostasis relies on the assembly and/or stability of large connexin 46 gap junction plaques on the broad sides of differentiating fiber cells. *Am J Physiol Cell Physiol*. 2015;308:C835–847.
83. Chandy G, Zampighi GA, Kreman M, Hall JE. Comparison of the water transporting properties of MIP and AQP1. *J Membr Biol*. 1997;159:29–39.
84. Gao J, Sun X, Moore LC, Brink PR, White TW, Mathias RT. The effect of size and species on lens intracellular hydrostatic pressure. *Invest Ophthalmol Vis Sci*. 2013;54:183–192.
85. Martinez-Wittinghan FJ, Srinivas M, Sellitto C, White TW, Mathias RT. Mefloquine effects on the lens suggest cooperative gating of gap junction channels. *J Membr Biol*. 2006; 211:163–171.
86. Costello MJ, McIntosh TJ, Robertson JD. Membrane specializations in mammalian lens fiber cells: distribution of square arrays. *Curr Eye Res*. 1985;4:1183–1201.
87. Costello MJ, McIntosh TJ, Robertson JD. Distribution of gap junctions and square array junctions in the mammalian lens. *Invest Ophthalmol Vis Sci*. 1989;30:975–989.
88. Buzhynskyy N, Hit RK, Walz T, Scheuring S. The supramolecular architecture of junctional microdomains in native lens membranes. *EMBO Rep*. 2007;8:51–55.
89. Buzhynskyy N, Girmens JF, Faigle W, Scheuring S. Human cataract lens membrane at subnanometer resolution. *J Mol Biol*. 2007;374:162–169.
90. Buzhynskyy N, Sens P, Behar-Cohen F, Scheuring S. Eye lens membrane junctional microdomains: a comparison between healthy and pathological cases. *New J Phys*. 2011;13:085016.
91. Scheuring S, Buzhynskyy N, Jaroslawski S, Gonçalves RP, Hite RK, Walz T. Structural models of the supramolecular organization of AQP0 and connexons in junctional microdomains. *J Struct Biol*. 2007;160:385–394.
92. Mangenot S, Buzhynskyy N, Girmens JF, Scheuring S. Malformation of junctional microdomains in cataract lens membranes from a type II diabetes patient. *Pflugers Arch*. 2009;457:1265–1274.
93. Ball LE, Little M, Nowak MW, Garland DL, Crouch RK, Schey KL. Water permeability of C-terminally truncated aquaporin 0 (AQP0 1-243) observed in the aging human lens. *Invest Ophthalmol Vis Sci*. 2003;44:4820–4828.
94. Zampighi GA, Eskandari S, Hall JE, Zampighi L, Kreman M. Micro-domains of AQP0 in lens equatorial fibers. *Exp Eye Res*. 2002;75:505–519.
95. Bassnett S, Wilmarth PA, David LL. The membrane proteome of the mouse lens fiber cell. *Mol Vis*. 2009;15:2448–2463.
96. Shiels A. Focus on molecules: major intrinsic protein. *Exp Eye Res*. 2012;101:107–108.

Investigative Ophthalmology & Visual Science